Temporal response of photodiodes with $GaAs/Al_xGa_{1-x}As$ ($0.1 \leqslant x \leqslant 0.3$) multiquantum well absorption regions

S. Goswami, L. Davis, and P. K. Bhattacharya
Solid State Electronics Laboratory, Department of Electrical Engineering and Computer Science, University of Michigan, Ann Arbor, Michigan 48109-2122

(Received 1 June 1992; accepted for publication 20 July 1992)

We have measured and analyzed the temporal response characteristics of high-speed photodiodes having $GaAs/Al_xGa_{1-x}As$ ($0.1 \leqslant x \leqslant 0.3$) multiquantum well absorption/transit regions. It is seen that the response time of devices with $Al_{0.1}Ga_{0.9}As$ barriers is fairly insensitive to the applied reverse bias and a 30-μm-diam mesa-etched device exhibits a 30 ps response time. The response time of devices with barriers having $x > 0.1$ is sensitive to the applied bias, which changes the mode of carrier escape from the wells for collections.

I. INTRODUCTION

Present day large bandwidth sources and optical fibers require fast photodetectors at the receiving end. *p-i-n* (or PIN) diodes have been commonly used for high-speed photodetection. Until recently, most PIN diodes utilized only the properties of bulk semiconductors. The optical properties of bulk PIN diodes are severely limited by the material used for the optically active region. It is well known that in quantum wells (QWs), the effective band gap of a material can be tuned by changing the well size, thus allowing one to modify the cutoff frequency in a high pass type device. Quantum wells display enhanced excitonic response and due to the quantum confined Stark effect (QSCE) the excitonic peaks display a quadratic variation with electric field.[1] Multiple quantum well (MQW) PIN diodes based on QCSE have been shown to be capable of discriminating between different wavelengths.[2,3] Another feature of QW diodes is the possibility of enhancement of carrier impact ionization ratio.[4-6] A higher impact ionization ratio can result in low-noise operation of avalanche photodiodes. Thus, *p-i*(MQW)*-n* photodiodes can potentially integrate the attributes of large bandwidth, spectral sensitivity, and low noise in a single device.

There are several recent reports on the temporal response of PIN photodiodes[7-9] with single-layer absorption regions and the detection bandwidth of the devices has been extended to the 100 GHz range.[9] The major factors limiting the response speed of these devices are the carrier drift time across the optically active intrinsic (absorption) region and the parasitics associated with the device mounting and packaging. The drift time can be reduced by using thin absorption regions. The transit delay is of the order of 5 ps for a 0.5 μm intrinsic region (assuming a carrier saturation velocity of 10^7 cm/s) and can be neglected for most diodes. In addition to these limitations, QW-based PIN diodes will have a delay associated with the carrier confinement in the quantum wells. This work focuses on the estimation of this delay along with optimization of the QW structure for better temporal response.

II. CIRCUIT MODEL

The optical response of photodiodes can be modeled by an equivalent circuit of the device and associated parasitics. The small-signal ac circuit model of a *p-i*(MQW)*-n* diode is shown in Fig. 1(a). The diode alone is modeled as a constant photocurrent source (I_{ph}) in parallel with a capacitance (C_D) and a series resistance (R_S). The device leakage resistance in parallel with the current source can be omitted, as this resistance is expected to be very high for reverse biased diodes. The parasitics associated with the diode and sample carrier are modeled as shown between the dashed lines in Fig. 1(a). At high frequencies, the bonding wires behave as transmission lines and the circuit model for parasitics is essentially a lumped representation of this. L_B's and R_B's are bond wires inductances and resistances, respectively. The capacitances associated with the bond wires are C_B and C_F. The measurement oscilloscope presents a 50 Ω termination and is shown as load, Z_0. The values for the circuit elements can be estimated from a one-port impedance measurement. The equivalent circuit for such a measurement is shown in Fig. 1(b) and is the circuit of Fig. 1(a) without the photocurrent source and the oscilloscope load. For optical-response considerations the circuit can be viewed as shown in Fig. 1(c), where the transforming network is the circuit of Fig. 1(b). The transfer function of this network can be expressed as

$$\frac{i_{ph}}{i_L}=\frac{1}{1+j\omega\, C_D R_C}\frac{Z_1}{Z_1+Z_B}\frac{Z_2}{Z_2+Z_0}, \quad (1)$$

where

$$Z_B=(R_{B1}+R_{B2})+j\omega(L_{B1}+L_{B2}), \quad (2)$$

$$Z_1=\left[j\omega\, C_B+\left(R_S+\frac{1}{j\omega\, C_D}\right)^{-1}\right]^{-1}, \quad (3)$$

and

$$Z_2=[(Z_1+Z_B)^{-1}+j\omega\, C_F]^{-1}. \quad (4)$$

In Eq. (1), i_L represents the load current.

III. EXPERIMENTAL TECHNIQUES

The device structure grown by molecular beam epitaxy (MBE) on semi-insulating GaAs substrate is schematically shown in Fig. 2. All the devices have the same structure except in the quantum wells, where the aluminum compo-

 © 1992 American Institute of Physics

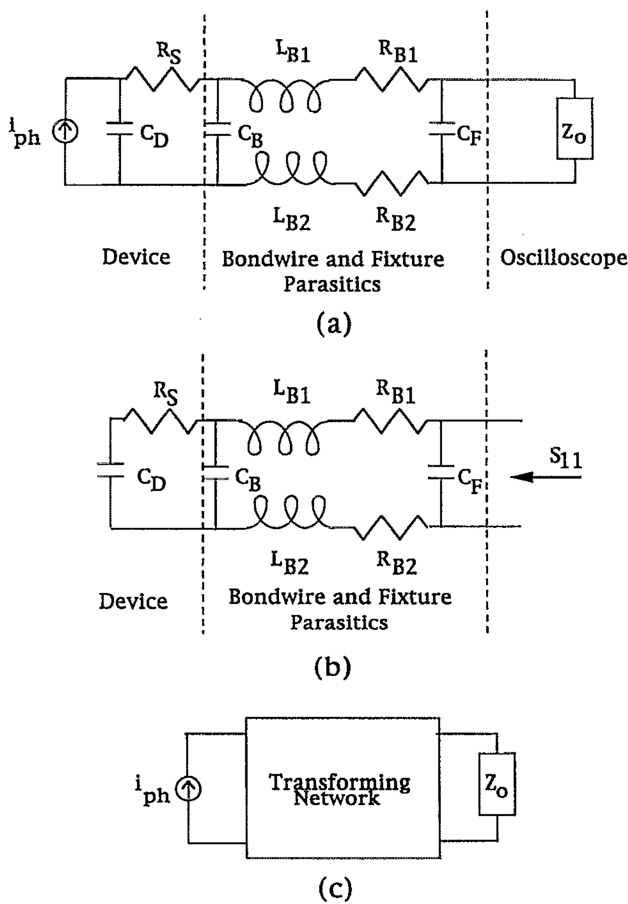

FIG. 1. (a) The small signal equivalent circuit of a *p-i*(MQW)-*n* diode and associated parasitic elements; (b) equivalent circuit for *S*-parameter measurement; (c) the diode equivalent circuit with current source and oscilloscope load with all the parasitic elements included in the transforming network.

sition in the barriers is varied, thereby varying the barrier height. The width of the well and barrier regions are kept constant at 80 and 90 Å, respectively. All samples have the same number of wells and hence the photogenerated carriers have to transit the same distance of undoped region.

0.05μm	p^+ GaAs	$5X10^{18}$ cm^{-3}
0.30μm	p^+ $Al_{0.4}Ga_{0.6}As$	$1X10^{18}$ cm^{-3}
0.02μm	$Al_xGa_{1-x}As$	undoped
Multiple Quantum Well	80Å GaAs well(30 wells) 90Å $Al_xGa_{1-x}As$ barrier(31 barriers)	undoped
0.02μm	$Al_xGa_{1-x}As$	undoped
0.30μm	n $Al_{0.4}Ga_{0.6}As$	$1X10^{18}$ cm^{-3}
0.40μm	n^+ GaAs	$5X10^{18}$ cm^{-3}
	Semi-insulating GaAs substrate	

FIG. 2. Schematic of layer structure for the *p-i*(MQW)-*n* photodetectors grown by MBE. In samples 1, 2, and 3, $x=0.1$, 0.2, and 0.3, respectively, in the $Al_xGa_{1-x}As$ barriers.

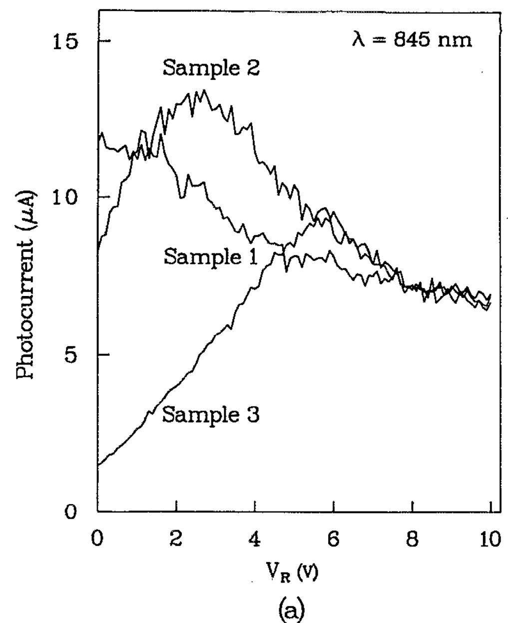

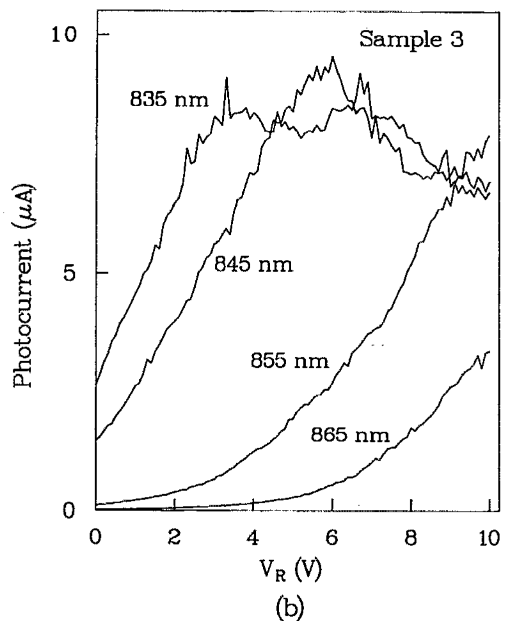

FIG. 3. (a) Measured photocurrent of the reverse biased diodes, and (b) photocurrent-bias characteristics of sample 3 at different wavelengths.

Measurements were made in three devices, in which the aluminum content (x) in the $Al_xGa_{1-x}As$ barriers of the MQW are 0.1 (sample 1), 0.2 (sample 2), and 0.3 (sample 3).

Device processing starts with wet etching of mesas down to the n^+ GaAs layer. The mesa is isolated by etching down to the semi-insulating substrate. Ohmic contacts to the p^+ and n^+ GaAs regions were made by depositing Pd/Zn/Pd/Au and Ni/Ge/Au/Ti/Au, respectively. The contacts were annealed at 450 °C for 3 min. 7000 Å of SiO_2 was deposited on the device for passivation and facilitation of bonding pad deposition. The fabricated devices were 30 and 90 μm in diameter. The reverse leakage current of the

TABLE I. Values for circuit elements obtained from microwave reflection measurements. The different elements are labeled in Fig. 1(b).

Sample	R_S (Ω)	C_D (pF)	C_B^a (pF)	R_{B1} (Ω)	L_{B1} (nH)	R_{B2} (Ω)	L_{B2} (nH)	C_F (pF)
1	65.0	0.09	0	1.7	1.4	1.7	1.1	0.17
2	52.0	0.12	0	2.1	1.8	2.1	2.1	0.15
3	50.0	0.21	0	0.9	1.3	1.0	1.0	0.15

[a]The bandwire capacitance C_B has values less than 1 fF.

devices is in the pA range.

The dc photoresponse of the devices was measured using a tunable dye laser pumped by a Nd:YAG laser as the excitation source. Figure 3(a) shows the photocurrent-voltage characteristics of the diodes for 845 nm excitation. The heavy-hole (HH) excitonic peaks of samples 2 and 3 are clearly visible at 2.8 and 6 V, respectively. The heavy-hole resonance of sample 1 is at a lower electron energy and therefore appears at a very low reverse bias. This change in the heavy-hole exciton energy is due to varying degrees of carrier confinement in the quantum wells. With higher aluminum content in the barrier, the carrier confinement increases and hence the corresponding exciton resonance energy increases. Figure 3(b) shows the photoresponse of sample 3 at four different excitation wavelengths. The heavy-hole peak moves toward higher reverse bias with increasing wavelength due to QCSE. Also, the light-hole (LH) peak is observed in the photoresponse at 835 nm, confirming the high quality of the quantum wells.

From capacitance-voltage measurements on 90-μm-diam devices, it was observed that the device capacitance is about 1.3 pF and the capacitance changes by about 25 fF for 3 V change in reverse bias. This change is considered negligible. The built-in potential V_{bi} effective in the MQW region can be estimated from the alignment of n-type and p-type $Al_{0.4}Ga_{0.6}As$ region Fermi levels. The calculated value of V_{bi} is 2.0 V, assuming the intrinsic carrier density of $Al_{0.4}Ga_{0.6}As$ to be 100 cm^{-3}.[10] Under these circumstances, it is reasonable to assume complete depletion of the i-(MQW) region even at low reverse biases.

IV. RESULTS AND DISCUSSION

The devices were mounted on high-frequency carriers for temporal measurements. These carriers are designed for operation upto 26 GHz and hence are expected to be suitable for the measurements. The S parameters of the mounted samples were measured with a HP8510 network analyzer. For our purpose only, the S_{11} parameter is relevant and is measured upto 10 GHz. The values of the elements in the equivalent circuit model is optimized to match the S_{11} data. These values are listed in Table I for the three samples. The light source for the temporal response measurements is a pulsed dye laser pumped with a modelocked Nd:YAG laser with a doubling crystal. The full width at half maximum (FWHM) of the dye laser pulses is less than 10 ps. A 0.25 m spectrometer is used for determining the excitation wavelength. To isolate the dc circuit from the ac circuit, a 26.5 GHz bias T is used. The

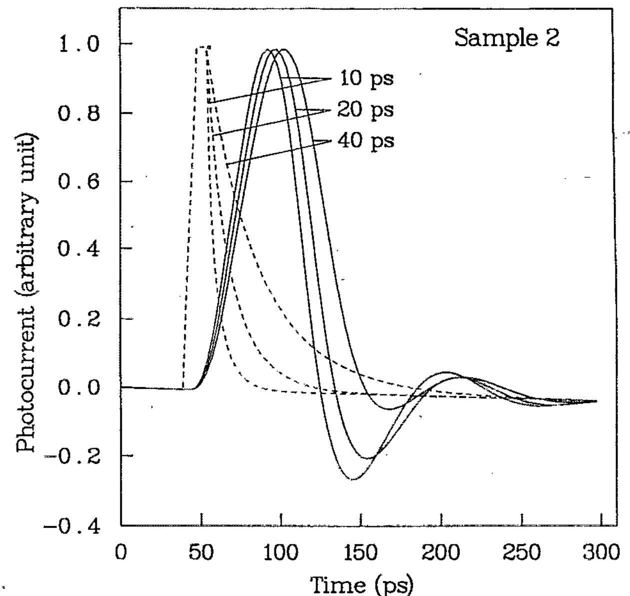

FIG. 4. Calculated response of sample 2 (solid lines) for excitation pulses of different decay times (dotted lines).

ac signal from the bias T is displayed on a high-speed sampling oscilloscope. A neutral density optical attenuator is used to adjust the beam intensity. The attenuator also helps in keeping the excitation in the small signal domain.

The optical excitation can be modeled as rectangular pulses of 10 ps duration without losing much accuracy. The optical pulses generate carriers in the quantum wells that subsequently escape and contribute to the photocurrent. For very short optical pulses, the photocurrent can also be approximated as a rectangular pulse of the same duration as the optical pulse but with an additional decay time, as shown by the dotted curves in Fig. 4. The additional fall time in the photocurrent results from the finite escape rate of carriers out of the quantum wells.[9] This current pulse is then modified by the device and carrier parasitics before being displayed on the oscilloscope. The amplitude of current pulses can be considered to be small enough to cause any perturbation of the electric field in the i-(MQW) region. Hence, only the dc bias is effective in band bending and the carriers in the quantum wells experience the same barrier over time. A fixed energy-band profile implies a time-invariant escape rate of carriers which, in turn, leads to an exponential decay of the photocurrent. As mentioned earlier, the transit delay in the 0.55 μm intrinsic region can be neglected. The solid curves in Fig. 4 shows the simulated oscilloscope traces for three different decay times (10, 20, and 40 ps). The circuit parameters of sample 2 are used for this simulation.

Figure 5(a) shows the experimental and simulated temporal responses of sample 1 ($x=0.1$ in the QW barrier) with 845 nm optical excitation. The solid curves represent experimental data for 1, 4, and 7 V reverse bias, which correspond to electric fields of 20, 73, and 127 kV/cm, respectively, in the MQW region. It is evident from this

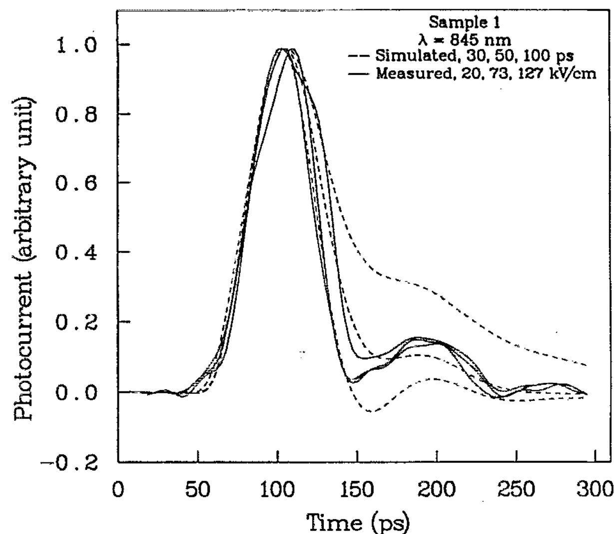

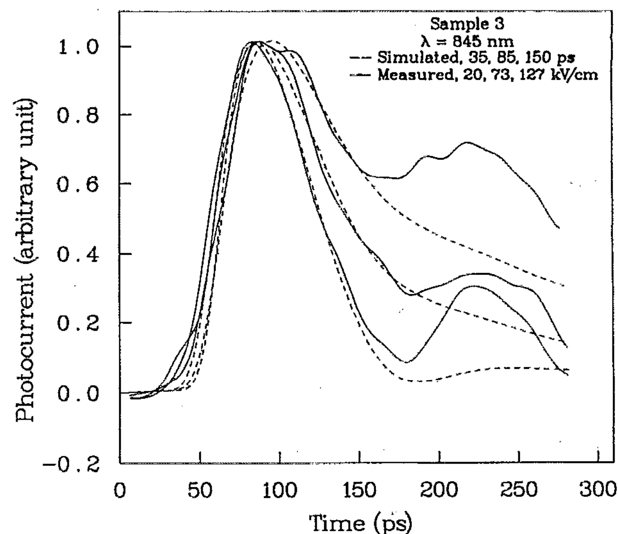

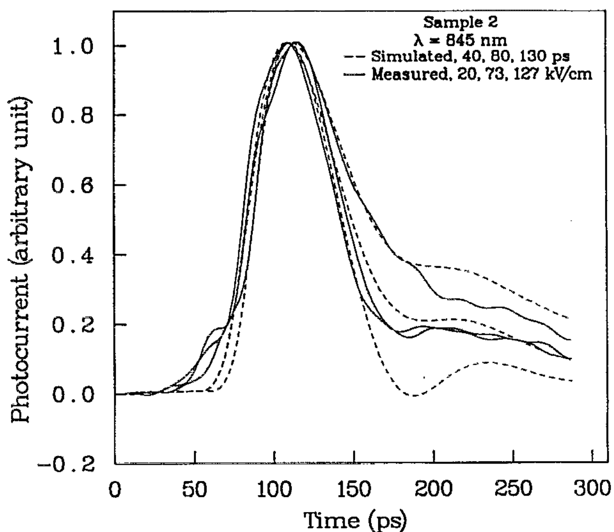

FIG. 5. Experimental (solid lines) and calculated (dotted lines) photoresponse at different biases and input pulse decay constants for (a) sample 1, (b) sample 2, and (c) sample 3.

figure that the device response does not improve appreciably with electric field. The dotted lines in Fig. 5(a) are the simulated responses with decay time constants of 30, 50, and 100 ps.

Figure 5(b) shows similar results for sample 2 with 845 nm optical excitation. Here the response changes appreciably from 1 to 4 V reverse bias. This is presumably due to the lower tunneling barriers seen by the carriers at higher electric field. The dotted curves in Fig. 5(b) correspond to 40, 80, and 130 ps decay times. Thus, with increasing electric field the intrinsic response of the device improves by a factor of 3, which also implies a three-fold increase of carrier escape rate. Temporal response characteristics of sample 3 with 845 nm excitation are shown in Fig. 5(c). The solid curves in the figure correspond to experimental results at 1, 4, and 7 V reverse bias and the dotted curves correspond to simulated responses with 35, 85, and 150 ps decay times.

From the above description, it is apparent that at high reverse bias the shortest (near-intrinsic) response times of devices 1, 2, and 3 are 30, 40, and 35 ps, respectively. Thus, at large reverse bias, the temporal characteristics of all the samples are similar. At small bias values, the decay constants for samples 1, 2, and 3 are 50, 80, and 150 ps, respectively. This could be understood qualitatively by considering the potential barrier height seen by the carriers for different AlGaAs barriers. The carriers in the QWs escape by thermionic emission or tunneling, or a combination of both.[11] At low bias and at room temperature, most of the photocurrent is due to thermionically emitted carriers, but at high bias, a major fraction of the photocurrent is due to tunneling.[2]

In the above, no distinction has been made between the escape rates of electrons and holes. Due to very different effective masses and density of states of electrons and holes and different band offsets, the carriers can be expected to have different escape rates. After dissociation of excitons, which has been shown to occur in subpicosecond times,[11] the electron and hole population in the QWs can be considered to be independent of each other. The instaneous photocurrent under this assumption is the superposition of the induced currents due to drift of electrons and holes.[12] In the limit of negligible drift time, the induced photocurrent can generally be approximated by the sum of two

decaying exponentials. The electric field in the QW region will be appreciably perturbed if the escape rates of the carriers are very different. As a consequence, the nature of the photocurrent will also be altered. Preliminary simulations indicate that the hole escape rates in these QWs are not too different from those of electrons.

V. CONCLUSION

In conclusion, we have measured and analyzed the temporal response of PIN photodetectors with MQW absorption regions having different barrier heights in the quantum wells. Devices with an $Al_{0.1}Ga_{0.9}As$ barrier in the MQW showed the fastest response and the response does not show appreciable dependence on bias. On the other hand, devices with an $Al_{0.2}Ga_{0.8}As$ and $Al_{0.3}Ga_{0.7}As$ barriers in the MQW indicate an appreciable bias dependence of the temporal response. The results strongly indicate that high-speed optoelectronic devices can be made with MQW absorption regions having small barrier heights and that such devices can be operated at low bias values without degrading their temporal response characteristics. Also, the excitonic features are preserved in the photocurrent-bias characteristics even at room temperature with $Al_{0.1}Ga_{0.9}As$ barriers.

ACKNOWLEDGMENTS

The authors acknowledge the help provided by P. Marsh and C. Kidner in microwave measurements. The work is supported by the Air Force Office of Scientific Research under Contract No. AFOSR-88-0168 and the Office of Naval Research under Grant No. N00014-90-J-1831.

[1] D. A. B. Miller, D. S. Chemla, T. C. Damen, A. C. Gossard, W. Wiegmann, T. H. Wood, and C. A. Burrus, Phys. Rev. B **32**, 1043 (1985).
[2] A. Larsson, P. A. Andrekson, S. T. Eng, and A. Yariv, IEEE J. Quantum Electron. **QE-24**, 787 (1988).
[3] S. Goswami, P. Bhattacharya, and J. Singh, IEEE J. Quantum Electron. **27**, 875 (1991).
[4] R. Chin, N. Holonyak, Jr., G. E. Stillman, J. Y. Tang, and K. Hess, Electron. Lett. **16**, 467 (1980).
[5] F. Capasso, W. T. Tsang, A. L. Hutchinson, and G. F. Williams, Appl. Phys. Lett. **40**, 38 (1982).
[6] F. Y. Juang, U. Das, Y. Nashimoto, and P. K. Bhattacharya, Appl. Phys. Lett. **47**, 972 (1985).
[7] J. E. Bowers and C. A. Burrus, J. Lightwave Technol. **LT-5**, 1339 (1987).
[8] C. Johnson, S. Sloan, D. Braun, J. L. Russel, M. Zurakowski, M. Lightner, F. Kellert, G. Patterson, R. Koo, D. Derickson, and J. Bowers, IEEE Trans. Electron. Devices **38**, 1968 (1991).
[9] Y. G. Wey, D. L. Crawford, K. Giboney, J. E. Bowers, M. J. Rodwell, P. Silvestre, M. J. Hafich, and G. Y. Robinson, Appl. Phys. Lett. **58**, 2156 (1991).
[10] S. M. Sze, *Physics of Semiconductor Devices* (Wiley, New York, 1988).
[11] A. M. Fox, D. A. B. Miller, G. Livescu, J. E. Cunningham, and W. Y. Jan, IEEE J. Quantum Electron. **QE-27**, 2281 (1991).
[12] G. Lucovsky, R. F. Schwarz, and R. B. Emmons, J. Appl. Phys. **35**, 622 (1964).